Engineering Geology 323 (2023) 107198

Contents lists available at ScienceDirect

Engineering Geology

journal homepage: www.elsevier.com/locate/enggeo

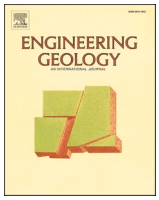

Combined electrical resistivity tomography and ground penetrating radar to map Eurasian badger (*Meles Meles*) burrows in clay-rich flood embankments (levees)

Adrian White [a,c,*], Paul Wilkinson [a], James Boyd [a,b], James Wookey [c], John Michael Kendall [d], Andrew Binley [b], Timothy Grossey [e], Jonathan Chambers [a]

[a] British Geological Survey, Nottingham, United Kingdom
[b] University of Lancaster, Lancaster, United Kingdom
[c] University of Bristol, Bristol, United Kingdom
[d] University of Oxford, Oxford, United Kingdom
[e] RSK Geophysics, Hemel Hempstead, United Kingdom

ARTICLE INFO

Keywords:
Electrical Resistivity Tomography
Ground Penetrating Radar
Meles meles
Burrow
Levee
Flood embankment

ABSTRACT

Globally, earth embankments are used to protect against flooding. Raised above the surrounding water table, these embankments make ideal habitats for many burrowing animals whose burrows can impact their structural integrity. Ground Penetrating Radar (GPR) is commonly used to identify and map animal burrows and other small cavities. However, the depth of investigation of a GPR survey can be severely limited in saline and clay-rich environments, soil properties commonly associated with flood embankments. In contrast, Electrical Resistivity Tomography (ERT) can image subsurface voids in conductive ground conditions but has been rarely used to image animal burrows. Here we aim to assess the efficacy of ERT and GPR to image two badger burrow networks, called 'setts', located in clay embankments on the River Ouse, Yorkshire, UK. The two setts were excavated to validate the geophysical results, and the soil was characterised through logging and geotechnical analysis to develop a ground model of the site. We find that ERT can accurately resolve tunnels down to 1.5 m depth, map the structure of a multi-entrance badger sett and successfully identify the end of the tunnels. This result compares favourably to the GPR surveys, which mapped all but the deepest tunnels, limited by its penetration depth due to clay soils. Our results show that ERT can be used as a primary survey tool for animal burrows in clay-rich environments and can be validated using co-located GPR surveys if penetration depth is sufficient. The implications of this study may allow embankment managers to map burrow networks, assess flood embankment stability, minimise repair costs, and reduce unexpected failures during flood events. Additionally, a better understanding of how, for example, local heterogeneities impact badgers' burrow geometry may be achievable using these geophysical methods, as they provide a non-destructive, repeatable method for imaging setts.

1. Introduction

Flood embankments (levees or dykes) are found in low-lying areas worldwide, protecting homes, industry and farmland from flooding caused by extreme weather events and tidal surges. However, these natural events are becoming more intense and frequent, so they increasingly test flood defences with higher water levels (IPCC, 2014). Additionally, the number of people living in areas at risk of flooding is increasing (Tellman et al., 2021). Combined, these factors increase the risk of disruption and potential loss of life in the event of a flood embankment failure. Thus, minimising failure risk is essential.

Flood embankments can be damaged by burrowing animals such as Eurasian badgers, beavers, rabbits, ground squirrels, groundhogs, coypus, American signal crayfish, and termites (Booth, 2019; Ceccato et al., 2022; CIRIA et al., 2013; Gilvear and Black, 1999; Taccari and van der Meij, 2016; Xu et al., 2010). Flood embankments can make suitable habitats for these animals as they are often inaccessible to people, have tall vegetation providing the animals cover, and can be well-drained, being raised above the surrounding water table (Fig. 1A) (Byrne et al., 2012; Macdonald et al., 2004; Remonti et al., 2006; Virgós and

* Corresponding author at: British Geological Survey, Nottingham, United Kingdom.
E-mail address: adwh@bgs.ac.uk (A. White).

https://doi.org/10.1016/j.enggeo.2023.107198
Received 10 March 2023; Received in revised form 23 May 2023; Accepted 24 May 2023
Available online 29 May 2023

Casanovas, 1999). Spatial correlations between animal burrows and embankment failures are well documented (Environment Agency, 2016; Gilvear and Black, 1999; Orlandini et al., 2015). For example, during the 1997 flood on the River Tay, Scotland, 66% of failures were associated with rabbit burrows (Gilvear and Black, 1999). This correlation is not surprising; burrows can reduce the length of the seepage path, which may result in a piping failure (Fig. 1B) (CIRIA et al., 2013, p. 167), burrows can collapse, causing preferential overtopping and finally, the embankment can saturate faster increasing the likelihood of shallow slope failures (Fig. 1C).

To mitigate the impact of burrowing animals, embankments must be remediated, prioritising sites with the highest failure risk. To assess the failure risk, three features of the burrow network must be known: 1) the extent of the burrows, 2) the position of the burrows with respect to the embankment, and 3) how they interconnect (Balistrocchi et al., 2021; Dassanayake and Mousa, 2020; Palladino et al., 2020; Taccari and van der Meij, 2016). However, for badger burrows, known as 'setts', determining their spatial extent is impossible from surface observations alone (Fischer and Dunand, 2016).

To map the spatial extent of a burrow with a geophysical method, a signal of the burrow must be detected and traced spatially. Two commonly used methods are Ground Penetrating Radar (GPR) (e.g. Borgatti et al., 2017; Nichol et al., 2003; RSK, 2020) and, less frequently, Electrical Resistivity Tomography (ERT) (Baccani et al., 2021; Borgatti et al., 2017; Butler et al., 1994; Environment Agency, 2015; Wilkinson et al., 2018). Other techniques, including electromagnetic induction and infrared remote sensing, have been tried with some success (Borgatti et al., 2017). Baccani et al. (2021) trialled Muon radiography to map burrows within the body of a levee. It could detect the burrowed region but is limited by the need for the tunnels to be between the detector and the source of muons from space.

GPR is commonly used for imaging animal burrows, including those dug by badgers (Borgatti et al., 2017; Nichol et al., 2003; RSK, 2020; Wisniewski et al., 2019), gopher tortoises (Kinlaw and Grasmueck, 2012), pocket gophers (Cortez et al., 2013), wombats (Browne et al., 2021; Swinbourne et al., 2016; Swinbourne et al., 2015), moles (Allroggen et al., 2019; Saey et al., 2014), rabbits (Stott, 1996), termites (Xu et al., 2010) and other small mammals (Chlaib et al., 2014). However, the depth of investigation of a GPR survey can be severely limited in saline and clay rich environments (Dunbar et al., 2007; Jol, 2009, p. 7), environments commonly associated with flood embankments (Dyer and Gardener, 1996), which may prevent the detection of even the shallowest burrows.

ERT has been widely used to detect sub-surface cavities due to the significant resistivity contrast between air and the surrounding material (e.g. Martínez-Pagán et al., 2013). However, there has been limited use on small scale voids, particularly those dug by animals. Butler et al. (1994) used electrical resistivity profiling to image three badger setts, but the results are unclear as the tunnels coincided with low resistivity anomalies, which is inconsistent with air-filled voids. ERT has been used to image regions of burrowing within flood embankments (Baccani et al., 2021; Borgatti et al., 2017; Environment Agency, 2015; Wilkinson et al., 2018), but none have aimed to map an entire sett with ERT. Mapping a soil pipe network has been attempted with a very fine electrode spacing (0.225 m), but the centimetre-scale soil pipes were below the level of detectability (Leslie and Heinse, 2013).

GPR and ERT surveys are often collected and interpreted together in subsurface investigations (e.g. Burke et al., 2012; Carrière et al., 2013; Pellicer et al., 2012) and the laboratory setting (Satriani et al., 2010). Borgatti et al. (2017) is the only study we know of that has combined

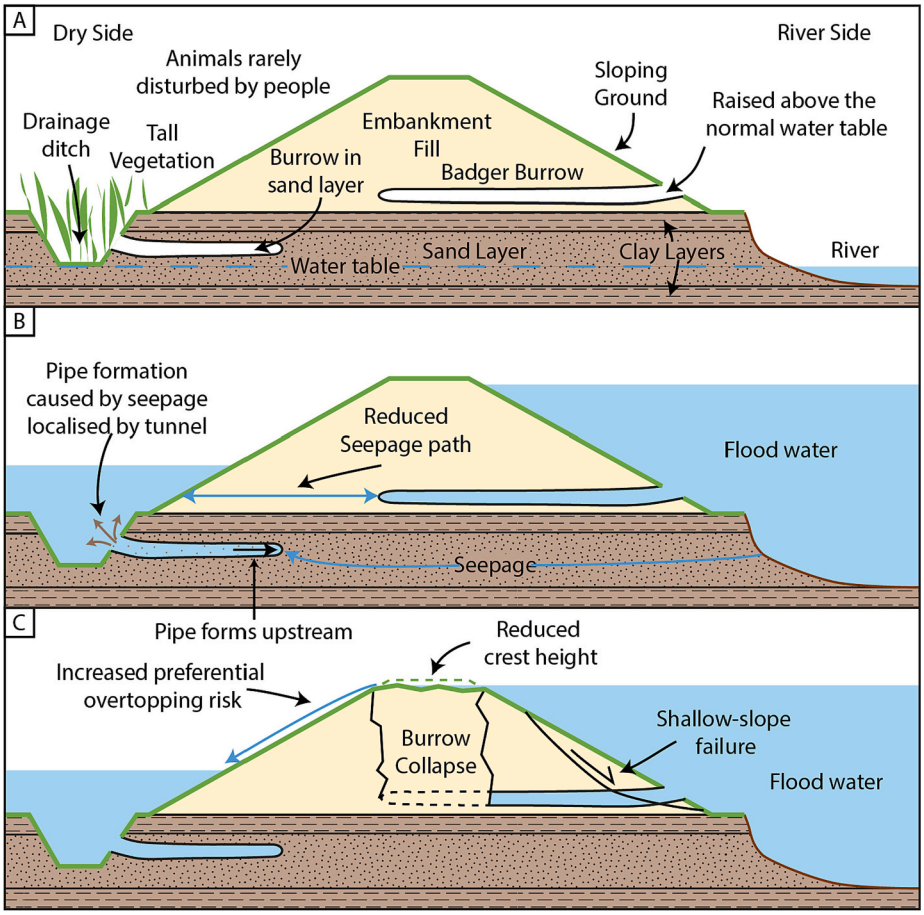

Fig. 1. Failure mechanisms associated with animal burrows in a typical flood embankment. A) Schematic earth embankment built on floodplain deposits. B) Seepage risk because burrowing animals shorten the seepage path (residual thickness); piping failure may occur if seepage rates are high enough to dislodge grains from non-cohesive soils. C) Structural failure of the embankment caused by burrow collapse, lowering the crest height and allowing for localised overtopping. Tunnels will shorten the saturation time, increasing the risk of shallow slope failure. © University of Bristol & British Geological Survey © UKRI.

ERT and GPR to image animal burrows; however, the agreement between the different survey methodologies is unclear.

To design a geophysical survey of a badger sett, details of the target (e.g. burrow dimensions and depth) are required to select the most appropriate method and settings and to assess whether the burrows could be detectable. Badger setts are characterised by multiple curving tunnels connecting to larger chambers (Roper et al., 1991). Tunnel dimensions are typically 30 ± 5 cm wide and 20 ± 5 cm high, with a domed roof and flatter base (Fischer and Dunand, 2016; Roper, 1992; Roper et al., 1991). The chambers are typically 50–60 cm in diameter and 45 cm high but may be smaller and can be located at the end of a tunnel or centrally joining multiple tunnels (Fischer and Dunand, 2016; Roper et al., 1991). Tunnels tend to drop steeply down from the entrance before running horizontally, generally between 0.5 and 1.5 m below the ground surface with none exceeding 2 m (Fischer and Dunand, 2016; Roper, 1992). Ideally, a useful survey technique should be able to detect/image a 30 cm wide air-filled void at depths of up to 2 m.

In this study, we aim to evaluate ERT and GPR for detecting and mapping badger burrows in clay rich environments. For the first time, we aimed to survey two badger setts in their entirety with ERT and GPR. Each sett located adjacent to flood embankments on a tidal section of the River Ouse (Fig. 2). Both badger setts had been identified by the Environment Agency (England's environmental regulator) for remediation, presenting a unique opportunity to compare the interpreted geophysical results with the excavated burrow network. Based on our results and published literature, we discuss implications for geophysics survey design to map badger setts and how this information could be used for flood embankment management.

2. Materials and methods

2.1. Case study location and survey details

Site 1 is located at the base of a barrier flood embankment near Wistow village, Yorkshire, UK (Fig. 2, 3A). The embankment is part of a flood retention reservoir set back from the river; this area can fill with water during flood events as part of a flood alleviation scheme (Fig. 3A). Site 1 has a single badger burrow entrance dug into the edge of the drainage ditch facing the embankment (Fig. 3B, C). The grass covered embankment (Fig. 3C) is mown several times a year and grazed by cattle. Before the survey, the grass was mown by the Environment Agency.

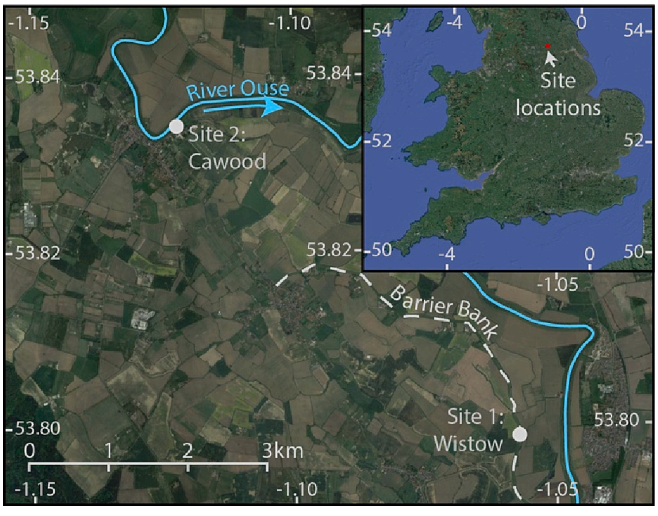

Fig. 2. Location map of the two badger setts reported in this study (with UK map inset). Both sites are located within flood embankments on the River Ouse downstream of York, Yorkshire, UK. Grid references in WGS84. Base map main map: ©2022 Google, Imagery ©2022 TerraMetrics, Map data ©2022. Inset map of England ©2022 Landsat / Copernicus, Data SIO, NOAA, U.S. Navy, NGA, GEBCO, Imagery ©2022 TerraMetrics, Map data ©2022 Google, GeoBasis-DE/BKG (©2009). © University of Bristol & British Geological Survey © UKRI.

Two geophysical methods, ERT and 250 MHz GPR, were deployed during a one day period by two people. Three hand augered holes were bored to depths between 1 and 1.5 m to characterise the structure of the site. No geotechnical analysis of the soil samples was carried out as visual analysis could easily distinguish the subsurface structure.

Site 2 is located on the river bank of the River Ouse in the village of Cawood, UK. (Fig. 2). The badger sett had four entrances on the riverside, 2 m from the embankment toe, located among the roots of four large willow trees (Fig. 4). The embankment rises 2.5 m above the surrounding land. The embankment and the riverbank are both formed of silts with clay and sand typical of floodplain deposits (Reading, 1986, chap. 3.6).

An initial geophysical survey was conducted by two people over two days, using 250 MHz GPR and ERT. Following the processing of the results, two months later, a four-day survey including 500 MHz and 800 MHz GPR, a second ERT survey and a geotechnical investigation was carried out. The follow-up survey aimed to investigate the resolution of the different techniques and characterise the site's stratigraphy. The measurements from co-located points in each ERT survey had similar values, so the results from the two surveys have been combined for clarity. The geotechnical investigation included two trial pits and a hand auger hole bored to 2 m deep. All recovered samples were visually similar, so participle size analysis, gravimetric moisture content and bulk density lab measurements were collected.

2.2. GPR

GPR surveys were carried out at Site 1 (Fig. 3) and Site 2 (Fig. 4), testing 250, 500 and 800 MHz antennae. These three antennas were selected to span the range of frequencies used for burrow surveys in the published literature (e.g. Chlaib et al., 2014; Nichol et al., 2003; Wisniewski et al., 2019). These antenna frequencies have a maximum vertical resolution of 2–7 cm (assuming a velocity of 0.07 m/ns), so they should be able to distinguish 30 cm-sized voids (Reynolds, 2011, chap. 13). The velocity was estimated using diffraction analysis, assuming each hyperbola was caused by a tunnel 0.3 m in diameter (Jol, 2009, chap. 5).

The initial 250 MHz GPR survey at both sites used a shielded 250 MHz antenna mounted on a Sensors and Software Incorporated pulseEKKO™ antenna mounted on a Pro SmartCart (Fig. 3C). A grid spacing of 50 cm was used in both parallel and perpendicular directions. The 500 and 800 MHz GPR survey at Site 2 used the shielded Mala ProEx 500 and 800 MHz antennas mounted on a sledge, with a grid spacing of 40 and 20 cm, respectively, in both parallel and perpendicular directions. Antennas with higher frequencies have higher resolution, but their signal attenuates faster, limiting their penetration depth (Chlaib et al., 2014). This trade off could be assessed using antennas with different frequencies. Attenuation of the 800 MHz GPR reduced its penetration depth to just 0.5 m, preventing it from detecting the badger sett, so it will not be discussed further.

All the GPR data was processed in ReflexW (Version 9.5.4) as 2D profiles following a standard procedure (Jol, 2009, chap. 5; Reynolds, 2011, chap. 13). The processing steps for the 250 MHz radargrams were: (1) each file was imported, correctly aligned to the local grid and any erroneous files were removed; (2) dewow filter was applied with a 4 ns window; (3) data collected before the start time was removed; (4) a Bandpass Butterworth filter with a low cut-off of 50 MHz and high cut-off 450 MHz was applied; (5) a background removal filter was applied to highlight hyperbola in the data; (6) an energy decay gain was applied to remove the effect of geometric spreading to enhance the reflections from greater depths; (7) a Kirchhoff migration was applied to the data using a constant velocity of 0.07 m/ns at both sites. The same processing steps were applied to the 500 MHz GPR, but at step 4, the Bandpass Butterworth filter used broader cut-offs of 125 MHz and 875 MHz,

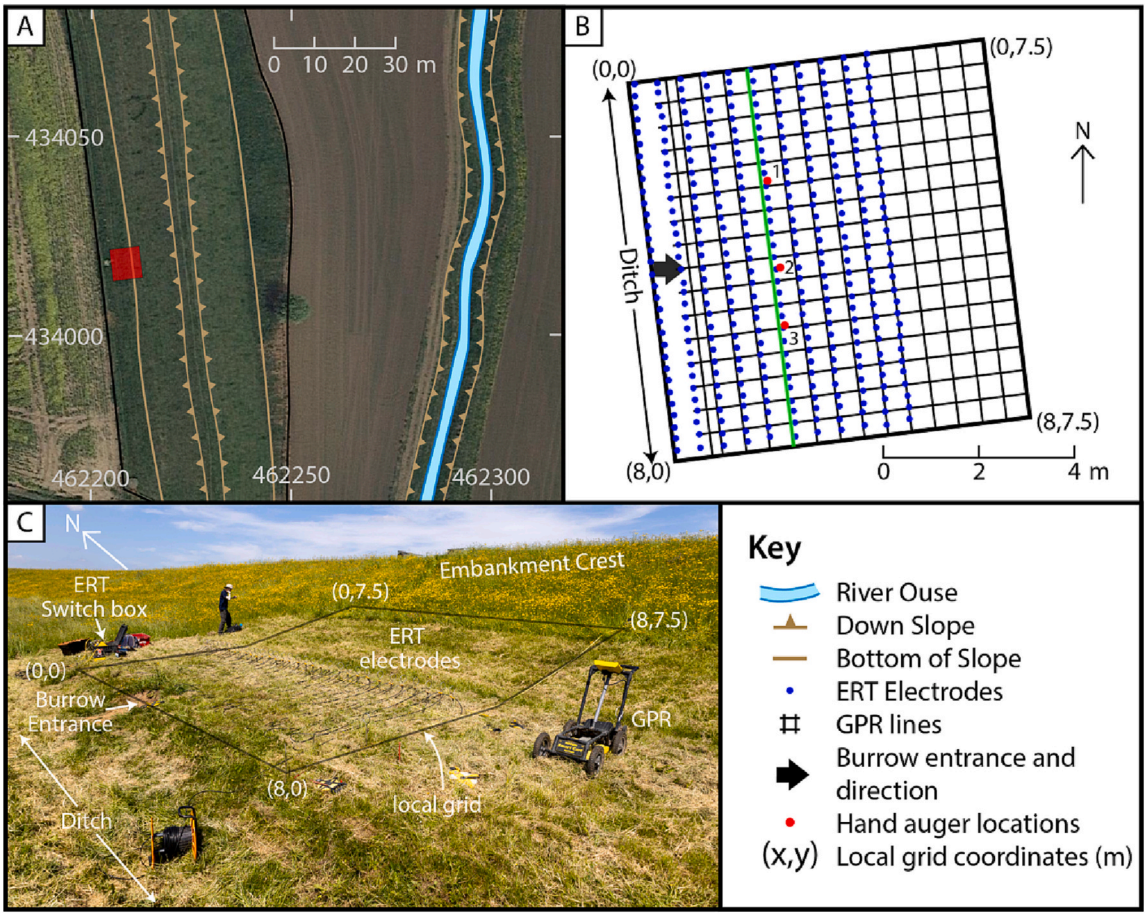

Fig. 3. Overview of Site 1 at Wistow, Yorkshire, UK. A) Location of the field site (red square) with respect to the flood embankment and the River Ouse. West of the red box is a pale dot indicating excavated soil from the burrow. B) Survey layout, including electrodes (blue dots), GPR profiles (black lines) and hand auger locations (red dots). The Black boundary box is the red box in A. Green line location of Fig. 5. C) Photograph of the site showing equipment and morphology. A) base map imagery ©2022 Google, Imagery ©2022 CNES / Airbus, Getmapping plc, Infoterra Ltd. & Bluesky, Maxar Technologies, Map data ©2022. © University of Bristol & British Geological Survey © UKRI. (For interpretation of the references to colour in this figure legend, the reader is referred to the web version of this article.)

respectively.

To map the sett, each radargram was visually inspected, and hyperbolas traced before the Kirchhoff migration was applied. Reflectors with similar characteristics, depth and reflection strength were also picked as they were assumed to be tunnels parallel to the survey line. Reflections interpreted as not part of the burrow network were not picked. The highest point of each hyperbola was extracted to infer the centre of the suspected tunnel roof. These maxima were then overlain on the migrated radargrams identifying the location of each anomaly. Each anomaly was then traced in the migrated data as it provided better separation of adjacent tunnels.

2.3. ERT

ERT data acquisition was carried out using parallel linear arrays of stainless-steel electrodes connected to an AGI SuperSting measurement instrument. The dipole-dipole array configuration was used for all measurements due to its suitability for a multichannel instrument resulting in short acquisition times (20 min for a 32-electrode line), ease of collecting reciprocal measurements for error modelling, no need for a remote electrode, and good lateral resolution for localised objects (Dahlin and Zhou, 2004; Gharibi and Bentley, 2005). For each survey line, the dipole-dipole configuration used dipole lengths of a = 1–4 electrode spacings and inter-dipole spacings na, where n = 1–8 (Loke et al., 2013, Fig. 2). For each four electrode measurement, a reciprocal measurement was made to estimate measurement error (Tso et al., 2017).

At Site 1, measurements were collected from 11 independent ERT lines spaced 50 cm apart, each with 32 electrodes spaced at 25 cm intervals (Fig. 3B). The mean contact resistance was 4080 Ω with a maximum of 6608 Ω. Site 2 covered an area eight times larger. The initial survey had alternating lines of 64 and 48 electrodes with 33 cm inter-electrode spacing and an inter-line spacing increasing from 33 cm close to the badger entrances to 100 cm further away to maximise spatial coverage while providing the highest resolution in the area of greatest complexity (Fig. 4). The follow-up survey at Site 2 used the same geometries and electrodes as Site 1 but with 17 parallel lines. Additionally, two lines of 32 electrodes spaced 100 cm apart were collected to place the sett in the wider embankment context (Fig. 4). At site 2, the mean contact resistance was 675 Ω with a maximum of 2067 Ω.

Data processing and filtering used the open-source software ResIPy (Blanchy et al., 2020). First, each line was processed to remove: all negative apparent resistivities, data with no reciprocal measurements, and measurements with reciprocal errors >20%. The reciprocal error was calculated for each measurement pair by dividing the difference between the forward and reverse measurements by their mean (Blanchy et al., 2020). Next, a power law error model was fitted to the data (Blanchy et al., 2020). Finally, measurements with <5% reciprocal errors were used in the inversion (Chambers et al., 2012). The average of the measurements was calculated for each reciprocal pair and then weighted based on the error model. At Site 1, 5676 reciprocal measurement pairs were collected, 77 (1.4%) were removed during data

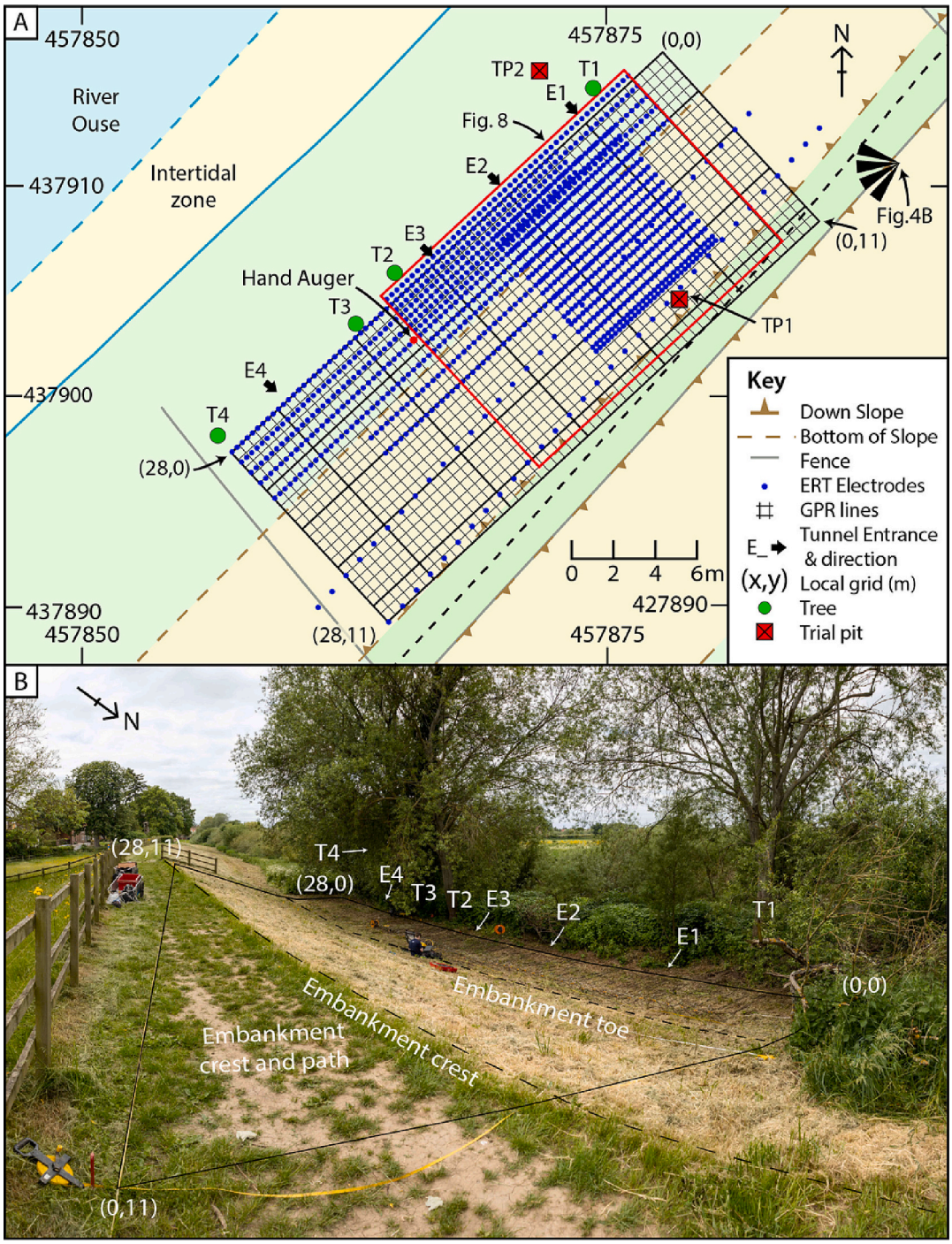

Fig. 4. Overview of Site 2 at Cawood, Yorkshire, UK. A) Site map showing the badger sett entrances (black arrows E1–4), large trees (green circles T1–4), 250 MHz GPR (black lines), ERT electrodes (blue dots), the ERT lines run NE SW. B) Photograph looking SW (panel A for location), showing details of the survey area. © University of Bristol & British Geological Survey © UKRI. (For interpretation of the references to colour in this figure legend, the reader is referred to the web version of this article.)

filtering. At Site 2, 22,996 reciprocal measurement pairs were collected, and 298 (1.3%) were removed during data filtering.

The ERT survey data presented were inverted using ResIPy, a software wrapper for R2 and R3t (Binley and Slater, 2020). All the data were inverted in 2.5D (called 2D for simplicity) and 3D using triangular and tetrahedral meshes, respectively. R2 and R3t use the finite element method to calculate a smoothness-constrained inverse solution (Binley and Slater, 2020). An L1 smoothness-constrained inversion in Res2DInv (v. 4.10.21) was tried as it was expected to better resolve the sharp air soil contrast of animal burrows (Supplementary Fig. 1). However, the L2 smoothness-constrained R2 inversion with a triangular mesh better distinguished individual tunnels, likely due to the finer mesh resolution (Loke et al., 2013). Each inversion aimed to converge with an χ^2 of 1.0 within 10 iterations (Binley and Slater, 2020), where χ^2 is a measure of the difference between modelled values and measured values, weighted according to errors (Binley and Slater, 2020; Günther et al., 2006).

The inverse model was imported into ParaView (v. 5.11.0) software to visualise the burrow structure and background geology. A threshold filter was applied to each ERT model to separate the resistive air-filled burrows from the surrounding ground along an isosurface. Picking an

appropriate resistivity value is crucial but has several challenges. Firstly, smoothness-constrained inversions, by definition, do not have sharp changes in resistivity, so there is no obvious threshold value to pick. Secondly, in heterogeneous ground, the resistivity of the surrounding soil changes, so the threshold value may need to vary across the site to isolate the burrow structure correctly. Thirdly, unrelated anomalies can be more resistive than those associated with the burrows, so they will be included when thresholding the model. Finally, the resistivity contrast of the burrow in the inverse model decreases with depth as the resolution of the ERT survey diminishes. With these challenges in mind, threshold values were iteratively tried until a reasonable burrow structure in keeping with expectations was achieved.

2.4. Positioning and ground truthing

A local grid was constructed at both sites using tape measures to lay out each survey accurately. Additionally, each electrode was surveyed, as was the start and end of each GPR line, and contextual information using a Leica RTK-dGPS with 2 cm horizontal accuracy. At Site 2, the dGPS signal was poor, so the local grid was used to infill points that could not be measured directly by the dGPS. The follow-up survey at Site 2 used that same local grid which was relocated using the GPS and by trying to re-occupying the peg holes made during the first survey.

Topographic data was provided by a Digital Terrain Model (DTM) for each site with a 1 m resolution. The DTM was the 2019 composite image from the Environment Agency derived from airborne LiDAR (Open

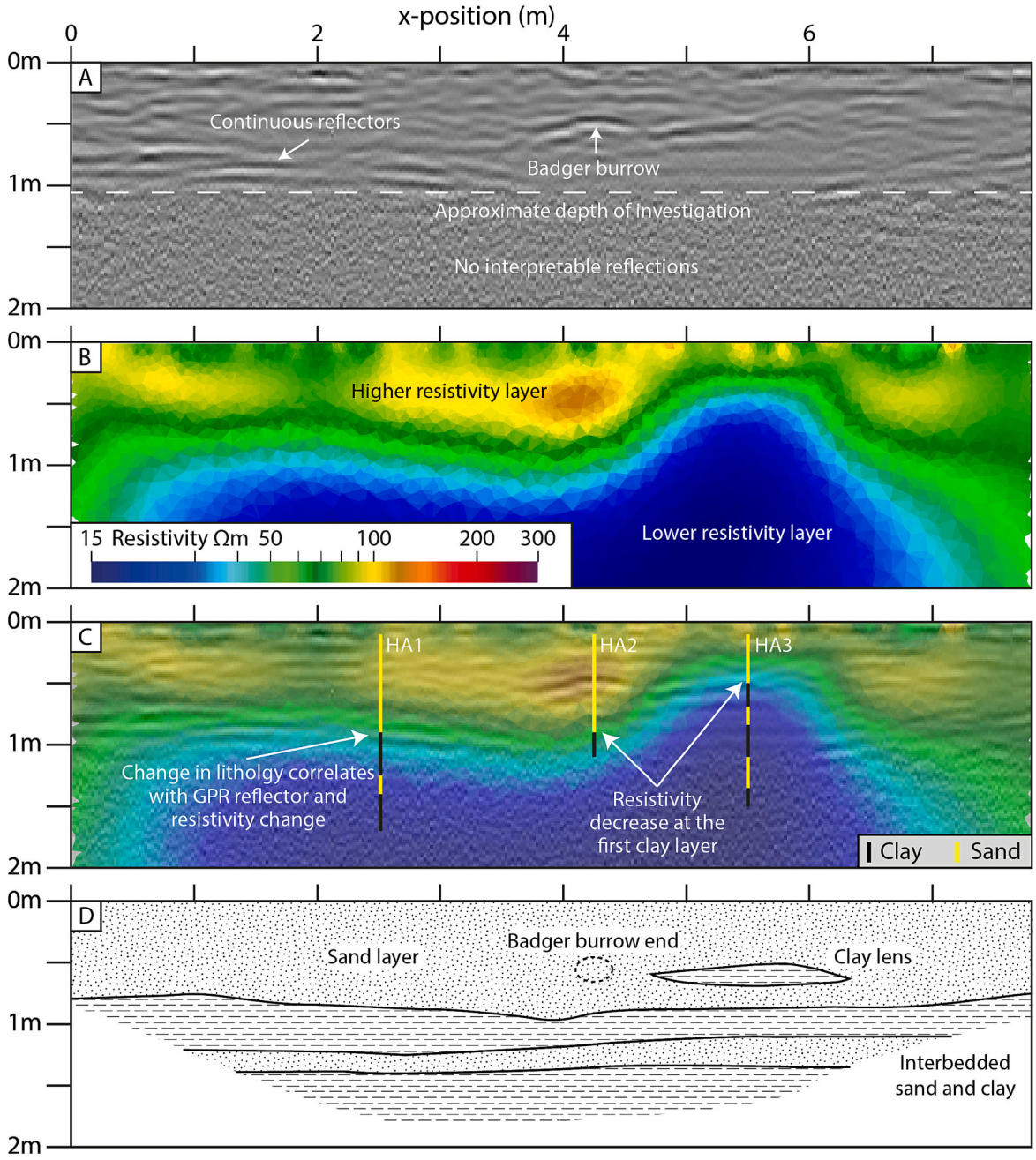

Fig. 5. Comparison of co-located ERT and GPR results at Site 1 at $y = 2.5$ m on the local Grid (Figs. 3). A) 250 MHz radargram. B) ERT slice from the 3D inversion. C) ERT model and GPR section overlain with hand auger logs. Yellow = Sand, Black = clay. D) Interpreted stratigraphic cross section using data presented in Panel C. © University of Bristol & British Geological Survey © UKRI. (For interpretation of the references to colour in this figure legend, the reader is referred to the web version of this article.)

Government License, https://environment.data.gov.uk/DefraData Download/). All measured x and y positions were draped onto this topography using a thin plate spline interpolation.

Soil composition and structure were assessed for each site using a combination of hand auger holes and trial pits. At Site 1, three holes were bored to depths between 1 m and 1.5 m (Fig. 3B, 5C). At Site 2, a single hole was completed to 2 m, and two trial pits were dug (Fig. 4A). Unlike at Site 1, all the soil samples at Site 2 were visually very similar, so particle size analysis, gravimetric moisture content, and bulk density were measured following British Standard ISO 1377 procedures to help interpret the geophysical data. After completing the survey, both sites were fully excavated by the Environment Agency, allowing maximum burrow extents to be recorded.

3. Results

3.1. Site 1 Wistow, Yorkshire, UK

The GPR survey at Site 1 has a depth of investigation of just over 1 m. An estimated skin depth of 2.27 m was calculated assuming a high-frequency regime, a resistivity of 100 Ωm and a relative permittivity of 18.4 (from the velocity estimate of the site) (Jol, 2009). The skin depth is greater than the depth of investigation due to clay layers at ~1 m that is not considered in the skin depth calculation. The site is characterised by relatively flat semi-continuous reflectors, below which little information is returned (Fig. 5A). Visual interpretation of the radargrams found a single hyperbola in each of the first five lines closest to the sett entrance (Figs. 5, 6). These hyperbolae align spatially with each other and the sett entrance. The orthogonal radargrams contain two strong reflectors connecting the hyperbola (Fig. 6). These GPR results suggest an approximately straight tunnel that is about 2 m long, with no side branches.

The 11 ERT lines were combined into a single 3D inversion, that converged within two iterations with an χ^2 of 1.03. The model is visualised as slices along each line of electrodes (Fig. 6A). The site is characterised by an upper 0.5 m - 1 m thick resistive layer, underlain by a lower resistivity layer (Figs. 5B and 6A). A 'ridge' of the low resistivity material extends from local coordinates (5, 1.5) on the local grid eastwards towards the embankment (Fig. 6A). Corresponding with the badger sett entrance, a resistive anomaly can be seen in each survey line back to $y = 2.5$ m on the local grid, where it becomes diffuse (Fig. 6A). To better visualise the tunnels, a threshold value of >120 Ωm was set (Fig. 6B) to define an opaque volume within the model. A lower threshold of 98 Ωm also produces a realistic burrow structure (Fig. 6C) but disagrees with the GPR data demonstrating the potential benefit of multiple techniques.

Hand augering revealed interbedded layers of clean fine sand and clay (Fig. 6C). The uppermost sand layer varies from 50 to 90 cm thick and is dry; in contrast, the sand layers below the clay layers are saturated. These deposits correlate with the Upper Pleistocene

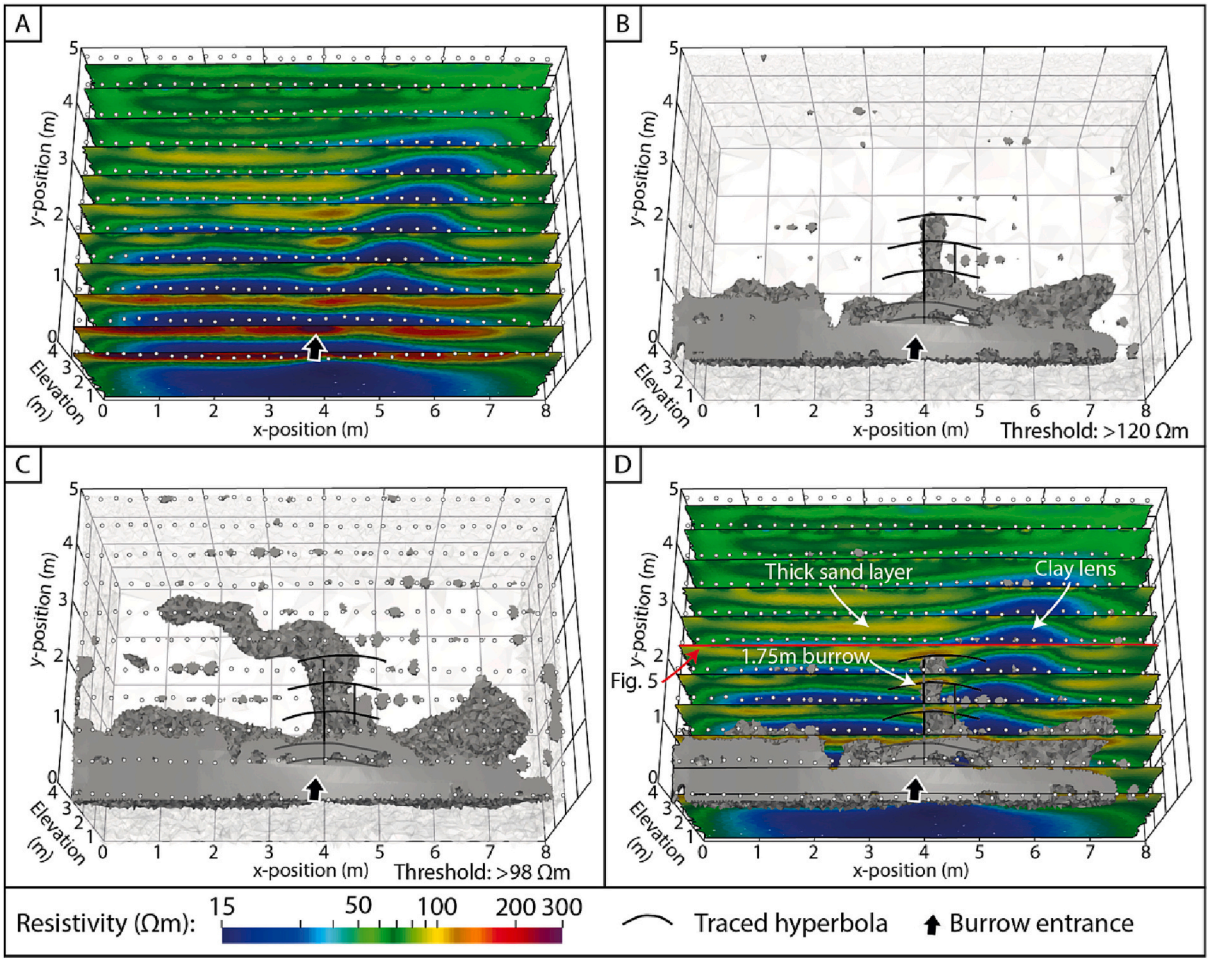

Fig. 6. 3D ERT results and interpretation of Site 1. A) 3D ERT inversion sliced along the electrode lines. B) The 3D inversion with a threshold applied at 120 Ωm, cells with resistivities below this threshold have a 10% opacity. ERT is overlain with traced GPR hyperbolas and reflections (black lines) for comparison. C) Same as B, but resistivity threshold set at 98 Ωm. D) Joint interpretation of the ERT and GPR combining panels A and B, showing the location of the tunnel, sand layer, and clay-filled channel. The red line in part D is the location of Fig. 5. © University of Bristol & British Geological Survey © UKRI. (For interpretation of the references to colour in this figure legend, the reader is referred to the web version of this article.)

glaciolacustrine deposits of the Hemingbrough Glaciolacustrine Formation transitioning up into the Breighton Sand Formation (Ford et al., 2004).

Excavation of the sett found that the single burrow entrance leads to a 1.75 m long burrow with no side branches. The burrow drops 25 cm over its length, with the burrow roof being 40 cm below ground level at the end of the burrow. Excavation of the tunnel found the diameter to vary. It is 30 cm in diameter at the entrance, narrowing to 25 cm before widening 60 cm from the burrows' end into a 30 cm wide, grass-filled chamber.

3.2. Site 2 Cawood, Yorkshire, UK

3.2.1. GPR

The 250 and 500 MHz antennas returned interpretable results from the top ~1.1 m, in keeping with an estimated skin depth of 0.91 m assuming a high-frequency regime, a resistivity of 40 Ωm and a relative permittivity of 18.4 (from the velocity estimate of the site). The radargrams from both antennas are visually very similar (Supplementary Fig. 1), possibly because both surveys have a measured dominant frequency of ~160 MHz. Only the results of the 250 MHz GPR survey are presented for conciseness and consistency between sites, and is referred to as GPR only.

The riverbank region has three distinct GPR facies (Fig. 7A). Facies 1 forms the top 0.5 m and exhibits undulating reflectors with clusters of small hyperbolae, interpreted as a soil layer disturbed by tree roots and small burrowing animals such as moles (Allroggen et al., 2019). Facies 2, between 0.5 and 1.1 m depth, has smaller amplitude background reflections punctuated by larger hyperbolas and reflections, interpreted as the badger sett. Facies 3 below 1.1 m is grainy and punctuated by large reflections; these reflections, if interpreted as hyperbolae, show moveout velocities compatible with diffractions in air. These hyperbolae were interpreted as airwave diffractions off the trees along the edge of the survey site. Each hyperbola crest approximately coincides with a tree trunk at 3.5 m and 16.5 m; this was unexpected as the antenna is shielded but is apparently common for lower frequency antennas on clay-rich ground (p.c. M. Stringfellow, RSK).

By picking the reflection and hyperbolas within facies 2 and interpreting the results a map of the badger sett was constructed (Fig. 8). Entrances 1–3 are connected and form a single badger sett, while entrance 4 (not shown in Fig. 8) had only two consecutive hyperbolae, matching the remediation results of a single, 1 m long burrow. The tunnels are shallowest close to the entrances and rapidly deepen, where the tunnels then connect and head into the embankment.

3.2.2. ERT

At Site 2, the 2D inversion of each line is presented rather than the 3D inversion (Fig. 9A). The 2D inversions converged within 2 or 3 iterations with an average χ^2 of 1.04 and a maximum of 1.32. A comparison of the 2D and 3D models, and a co-located radargram, found that the ERT inversions were similar, but the 2D models better resolve small resistive anomalies that match the hyperbolae in co-located radargrams. The reason for the better performance of the 2D inversion is unclear. 2D inversions can use a finer mesh, potentially better resolving the tunnels, and have one fewer spatial degree of freedom that may help localise anomalies associated with linear structures orientated perpendicular to the survey line. However, when using 2D surveys, inversion may contain artefacts where the 2D assumptions are violated, particularly offline topographic effects and tunnels running parallel to the survey line (e.g. Ball et al., 2022; Bièvre et al., 2018; Hojat et al., 2020).

The ERT inversions show resistive anomalies surrounded by lower resistivity material (Fig. 7B). The embankment and riverbank material below 1 m have similar resistivity values of 25–45 Ωm. To improve the visualization of these resistive anomalies, each 2D model was thresholded independently, working systematically away from the burrow entrances. The threshold value was picked to best visualise the tunnels. It was found that the threshold value on the riverbank could be set to 65 Ωm to image the burrow network while removing the surrounding material. On the embankment, the threshold value was lowered to between 45 and 50 Ωm (Fig. 9A). Finally, the top 30 cm of each line was

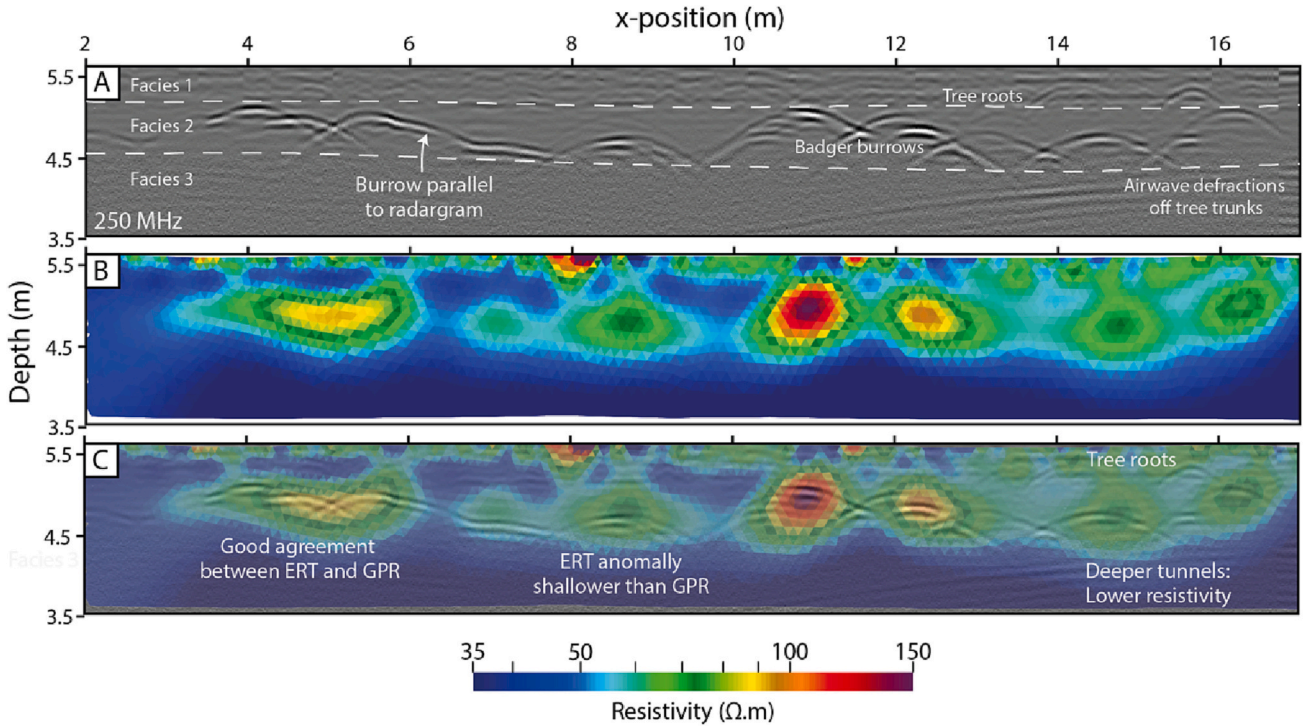

Fig. 7. Comparison of 250 MHz GPR radargram (A) with a co-located ERT model inverted in 2D with L2 smoothing (B) at Site 2, y = 1 m on the local grid. C) ERT model overlain onto the 250 MHz GPR data, showing the strong agreement between the two methods. For comparison with 500 MHz GPR, L1 ERT inversion and a 3D inversion, see supplementary Fig. S1 © University of Bristol & British Geological Survey © UKRI

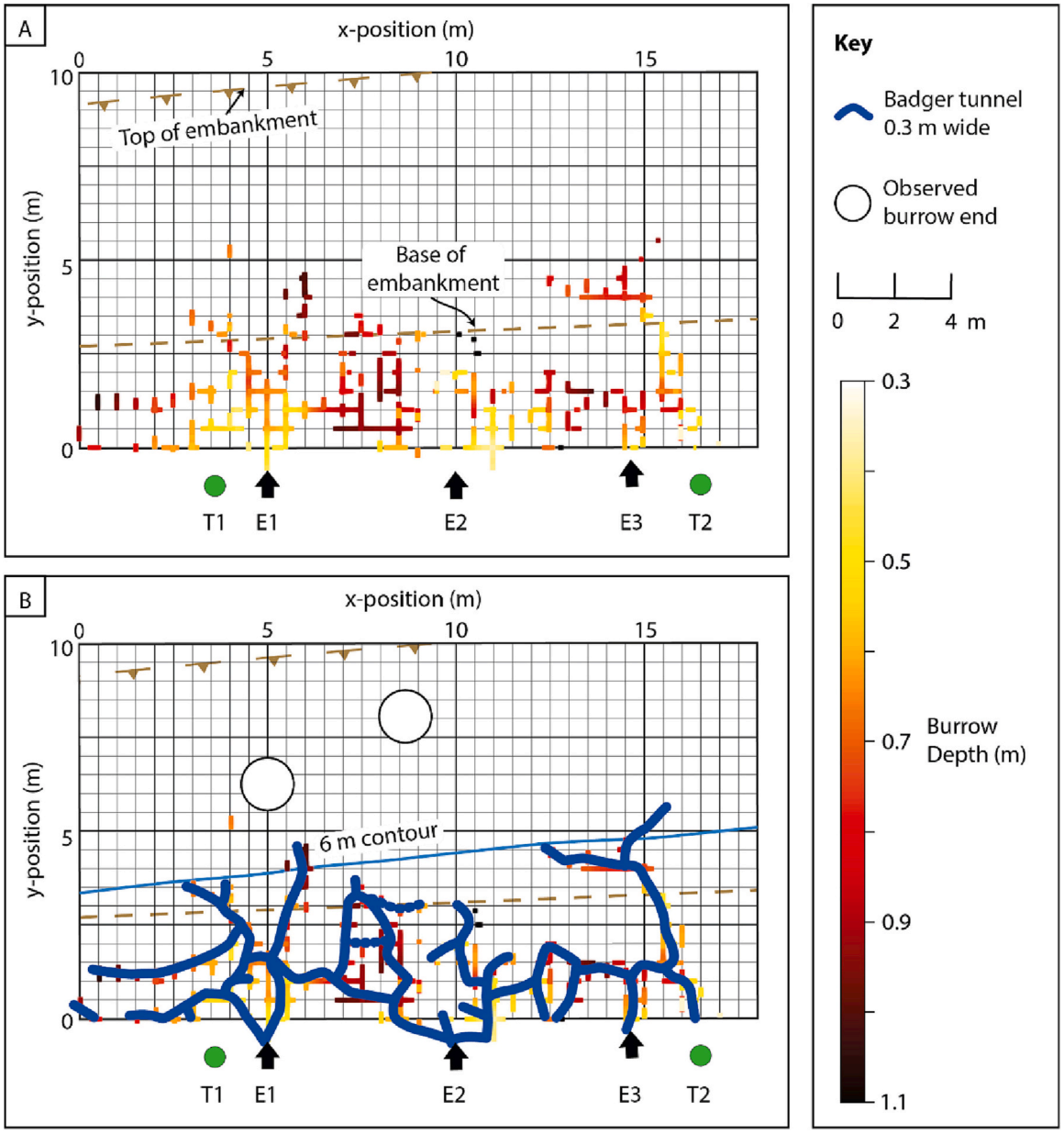

Fig. 8. A) Map of traced reflections at Site 2, picked from migrated GPR data, coloured with depth below the ground surface. B) The interpreted burrow network. GPR collection grid (black lines), badger sett entrances (black arrows E1–3), the large trees (green circles T1–2) and the white circles are maximum burrow extent from site excavation. The figure has been cropped at $x = 18$ m, beyond which very few hyperbolae were present. © University of Bristol & British Geological Survey © UKRI.(For interpretation of the references to colour in this figure legend, the reader is referred to the web version of this article.)

removed to remove distracting high resistivity anomalies close to the surface caused by roots, model artefacts and desiccated soil layer.

The lines closest to the burrow entrances have the largest resistive anomalies that can be traced from the burrow entrances through each 2D model towards the embankment (Fig. 9A). Entrances 1 to 3 have clear resistivity anomalies indicating a well-developed burrow network that extends close to the embankment crest, matching the end of the excavated sett. A small anomaly close to entrance 4 also supports the GPR that the tunnel does not extend far.

3.2.3. *Invasive observations*

All the samples had very similar particle size distributions with average values of 61% silt, 27% clay and 12% sand (Table 1). The soil from entrance 3 closely matched the soil horizon 0.65 m - 0.95 m depth in the hand auger sample. For each trial pit, undisturbed samples enabled bulk density measurements that also allowed porosity and saturation to be calculated assuming a grain density of 2.65 g/cm^3 taken from published literature (e.g., Chambers et al., 2014a, 2014b). The 2 m deep hand auger confirmed that the hyperbolae in GPR facies 3 were not caused by any soil interface and were offline artefacts.

Visual inspection of the sett was carried out during the remediation work. Entrance four led to a ~ 1 m long, partially collapsed burrow, confirming the geophysics results. Entrances 1–3 were connected by a complex tunnel network, with the furthest reaching ~8 m from the entrance and 1 m short horizontally of the embankment crest (Fig. 9B). The tunnels ran near horizontally into the embankment.

4. Geophysical data interpretation

4.1. *Site 1 Wistow, Yorkshire, UK*

A ground model of Site 1 was constructed by combining and

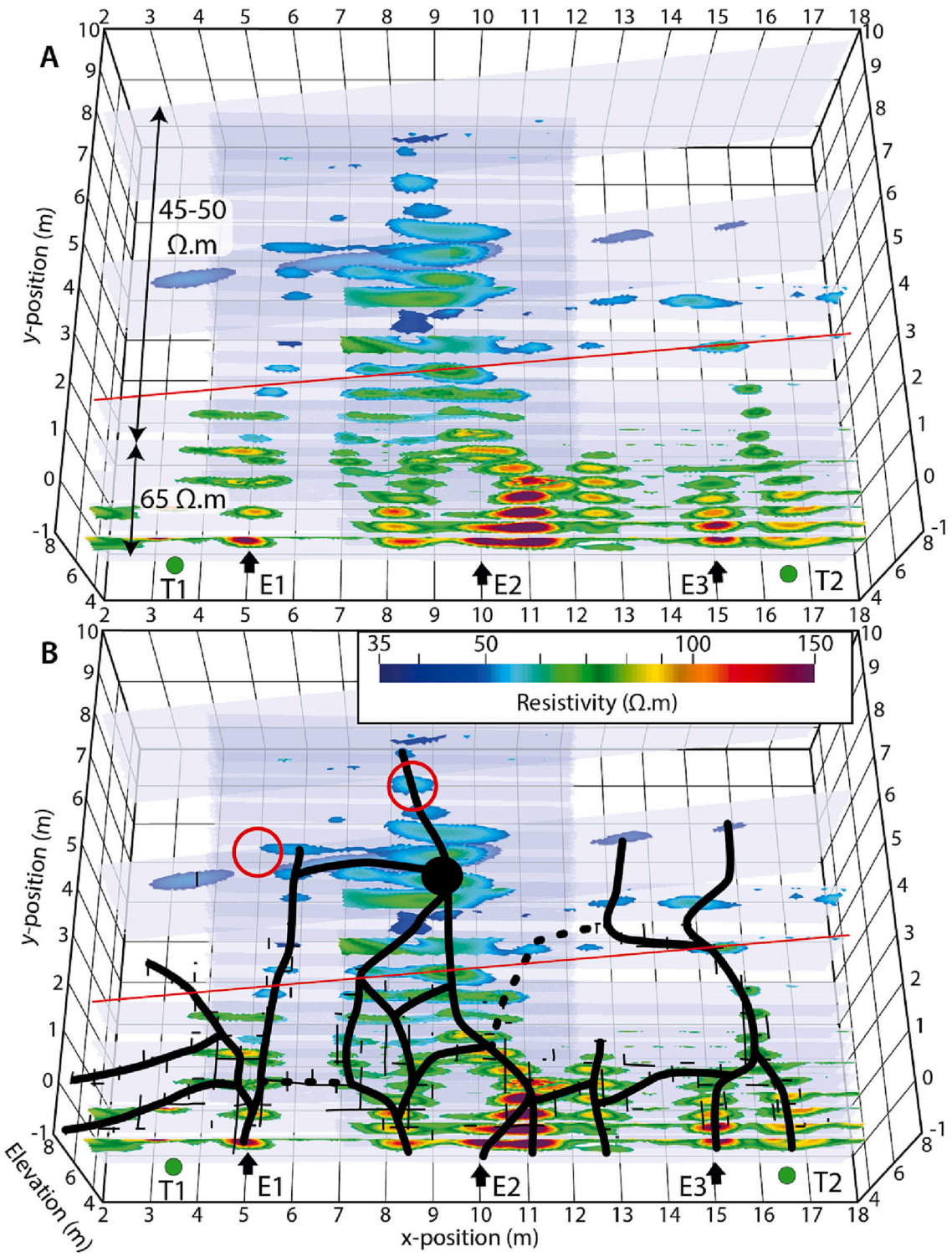

Fig. 9. Site 2 ERT results (A) with joint interpretation (B) of the ERT and GPR results (Fig. 8). Badger sett entrances (black arrows E1–3), large trees (green circles T1–2), approximate burrow terminations (red circles), and embankment toe (red line). In the interpretation the solid black lines are burrows and dashed are possible burrows. ERT Model cropped between 2 and 18 m where the burrows were present in the survey. © University of Bristol & British Geological Survey © UKRI. (For interpretation of the references to colour in this figure legend, the reader is referred to the web version of this article.)

interpreting the GPR, ERT, and intrusive information (Fig. 5, 6D). By comparing these data sets for a cross section at $y = 2.5$ m on the local grid (Fig. 5), the stratigraphy of the site was interpreted. The most prominent GPR reflectors correlate with the decreases in resistivity in the ERT model; this matches the appearance of the first clay layer (Fig. 5C). This correlation enables the auger logs to be extrapolated using the geophysical data establishing a detailed cross-section of the site (Fig. 5D). The low resistivity 'ridge' to the right of the burrow is caused by a small clay lens imaged by the GPR. The sand below the clay lens is not resolved in the ERT model. This lack of detectability is most likely due to current channelling in the clay lens masking the resistive sand below and the decreasing resolution of ERT with depth. The GPR,

Table 1
Geotechnical data from Site 2, location of each sample see Fig. 4. GMC = Gravimetric Moisture Content. © University of Bristol & British Geological Survey © UKRI.

Sample	Particle size analysis (%)			GMC (decimal)	Bulk density g/cm3	Porosity (%)	Saturation (%)
	Clay	Silt	Sand				
TP1 Embankment Core	22.98	64.73	12.29	0.200	1.520	0.426	0.713
TP2 River bank	31.80	58.54	9.66	0.224	1.105	0.583	0.425
Sett Entrance 3	26.91	58.79	14.30	0.255	–	–	–
Hand auger mean	27.65	60.80	11.55	0.290	–	–	–

by contrast, can image through the clay lens and pick out a continuous clay layer at 0.9 m depth; below this, little information is returned. Based on the 3D ERT model, we can interpret the clay lens as a clay-filled channel parallel to the badger tunnel (Fig. 6D). Along the edge of the ditch, the higher resistivity material is rubble dumped along the embankment edge, partly infilling the ditch.

The joint 3D interpretation of the site confirms that the burrow imaged by the GPR and visualised in the ERT model thresholded at 120 Ωm match the excavated burrow very closely. Additionally, the ERT with the 120 Ωm threshold has imaged the geometry of the tunnel showing it narrowing before widening into the chamber at the end (Fig. 6B). The 98 Ωm threshold was too low and included sand around the outside of the burrow and the continuation of the sand lens through which the badgers dug. This demonstrates the benefits of combining multiple geophysical methods. However, in the absence of supporting data to verify the true tunnel length in the ERT model, the width of the thresholded tunnel can be considered, the 120 Ωm threshold produced a tunnel 30 cm wide, a realistic diameter.

4.2. Site 2 Cawood, Yorkshire, UK

Different threshold values were used for interpreting the ERT model for the embankment and riverbank areas. The embankment soil has a lower resistivity, and the tunnels are deeper (Fig. 9A). A difference in soil composition cannot explain the lower resistivity of the embankment soil, as its lower clay content would normally increase resistivity (Waxman and Smits, 1968) (Table 1). However, the embankment soil has been mechanically compacted during construction, increasing the bulk density to 1.520 g/cm^3 and decreasing its porosity, while the bulk density of the natural riverbank is 1.105 g/cm^3 and has higher porosity. The same gravimetric moisture content is observed across the site, so the lower porosity embankment material is more saturated so has a lower resistivity (Archie, 1942). This demonstrates that in environments containing natural and manmade features the assumptions of constant porosity for monitoring moisture dynamics cannot necessarily be relied upon due to differential compaction (e.g. Chambers et al., 2014a, 2014b; Tresoldi et al., 2019).

A joint interpretation of the GPR and ERT results for the cross-section at $y = 1$ m (local grid) shows excellent spatial agreement between the hyperbolae and reflectors, and the resistivity anomalies (Fig. 7C). A full 3D joint interpretation (Fig. 9B), of the GPR data (Fig. 8A) and the thresholded resistivity sections (Fig. 9A), allows the badger sett to be mapped. This is a qualitative interpretation, and there is some uncertainty in this burrow network, particularly in joining burrow anomalies between each survey line. In the riverbank region and into the toe of the embankment, the interpreted tunnel network is robust due to the excellent correlation between the picked GPR hyperbolae and the thresholded resistivity anomalies. Beyond the embankment toe, there is significantly more uncertainty in the picked burrow network as the burrows are too deep for the GPR to detect, and the ERT resistive anomalies are smaller and more diffuse.

To evaluate the depths of the tunnels, the centre of each resistive ERT anomaly and the peak of each GPR hyperbola was picked and projected onto the y position (Fig. 10). There is good agreement between the GPR and ERT depths; as expected, the GPR is slightly shallower as GPR detects the tunnel roofs, while ERT images the whole tunnel. From the tunnel entrances at $y \approx -0.5$ m, the tunnels gradually drop over the first 2 m before climbing for the rest of their length, gaining over 1 m in height (Fig. 10). While the tunnel depths show some undulations (Fig. 9A) and deepen towards the embankment, they also partially follow the topography (Fig. 10), contrasting with excavated setts that are horizontal (Roper, 1992; Roper et al., 1991).

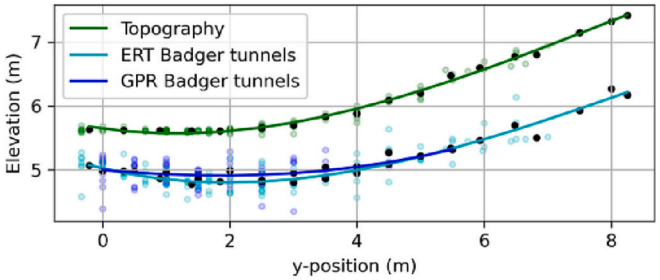

Fig. 10. Plot of average tunnel depth from the sett entrance (light blue: ERT, dark blue: GPR). The x-axis is the y-position of the local grid (Fig. 4), and the embankment elevation is shown in green. The ERT tunnel depth is the midpoint of each resistive anomaly. The GPR tunnel depths were from the top of each GPR hyperbola. The black dots are the average elevation at each half metre interval along the y-position of the local grid. © University of Bristol & British Geological Survey © UKRI. (For interpretation of the references to colour in this figure legend, the reader is referred to the web version of this article.)

5. Discussion

5.1. ERT survey design for badger setts

Optimising ERT survey design is essential for maximising the return signal from the tunnels while minimising acquisition time. Key survey parameters that can easily be changed are electrode spacing and array type. Dipole-dipole arrays are commonly selected for 3D surveys (e.g. Chambers et al., 2012; Leslie and Heinse, 2013) and for animal burrows (Baccani et al., 2021; Borgatti et al., 2017). Electrode spacing can easily be changed making it the obvious variable to consider. However, there is no agreement on the best electrode spacing, with spacings of 0.25–1.5 m used on badger setts in the published literature (Baccani et al., 2021; Borgatti et al., 2017; Butler et al., 1994; Wilkinson et al., 2018). Gharibi and Bentley (2005) suggest electrode spacing should be smaller than the minimum target size, so a 25 cm electrode spacing should be used for badger sett surveys, as we used at Site 1. At Site 2, the 1 m spacing survey imaged multiple tunnels, confirmed by the 25 cm spacing survey, despite the tunnels being much smaller than the electrode spacing (Fig. 9A).

To determine the most appropriate electrode spacings, the ERT line at Site 2, $y = 0$ m, was selected (Fig. 11). This survey line contains 48 electrodes with an electrode spacing of 0.33 m. The tunnels are mostly relatively close to the surface, although there is a deeper tunnel for comparison. The data was downgraded to simulate 0.67 m and 1 m

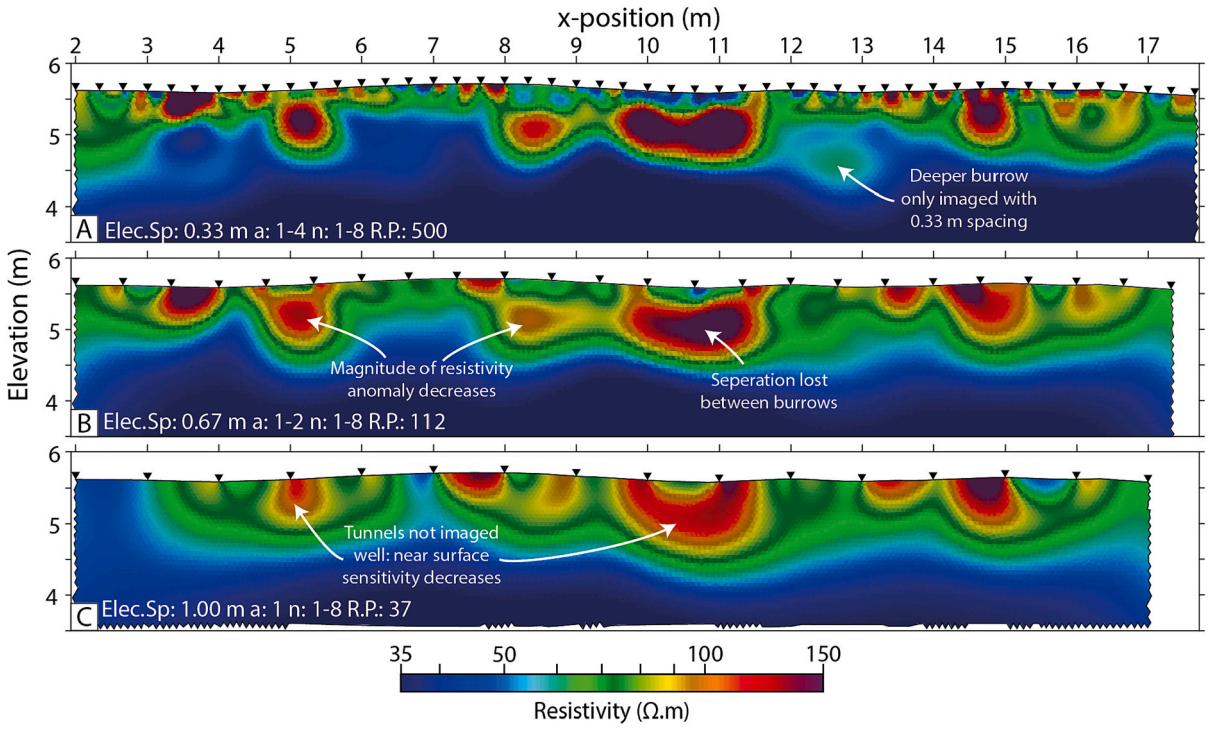

Fig. 11. 2D inversion of ERT line at Site 2, $y = 0$ m. A) Original survey with 48 electrodes spaced 0.333 m apart. B) Degraded data with every second electrode, creating a survey of 24 electrodes spaced 0.667 m apart. C) Degraded data with every third electrode, creating a survey of 16 electrodes spaced 1.00 m apart. R.P. = Reciprocal Pairs. © University of Bristol & British Geological Survey © UKRI.

electrode spacing by keeping measurements that only used every second and every third electrode, respectively. Degrading the electrode spacing also degrades the survey parameters by removing electrodes from the data. The initial surveys had a range of dipole lengths from $a = 1$–4; this reduces to $a = 1$–2 for the 0.67 m survey and $a = 1$ for the 1 m survey. This degradation of the measurement set will mean that the resulting models will be worse, particularly at greater depths, compared to those resulting from the complete measurement set.

Increasing the electrode spacing impacts the imaging of the tunnels in three ways. Firstly, it decreases the magnitude of the resistivity anomaly associated with each tunnel, as the survey becomes less sensitive to small anomalies making them harder to detect (Fig. 11). Secondly, the definition between closely spaced tunnels is lost (Fig. 11B). Thirdly, tunnels close to the surface are poorly imaged due to lower surface sensitivity (Fig. 11C). However, the 1 m electrode spacing performs remarkably well and could survey a line three times longer in the same acquisition time. Fig. 11C only contains 37 reciprocal pairs, demonstrating how few measurements are needed to detect the presence of tunnels – an optimised survey could significantly reduce survey time (Wilkinson et al., 2006).

5.2. Visualising burrows in ERT data

Animal burrows have sharp boundaries between their air-filled void and the surrounding soil. However, the R2 and R3t inversion codes use a finite element method to calculate an L2 smoothness-constrained inverse solution. While these inversions have successfully imaged the burrow network, they could be improved in several ways. 1) The burrow walls are not resolved in the ERT model with a sharp boundary. 2) The resistivity values of the air-filled burrows are much closer to that of the resistivity surrounding material than to air.

The methodology chosen to invert and visualise the ERT data can be selected to better resolve a burrow network. For example, in the methodology, a comparison between the L1 and L2 smoothed inversion techniques is made, as L1 inversion can include sharper changes in resistivity so in some cases may better resolve the tunnel boundaries. Similarly, identifying the tunnel boundaries can be done using several methodologies, this study threshold the ERT models to separate the resistive anomalies associated with the burrows; other methods include, for example, identifying the steepest resistivity gradients within the ERT model (Chambers et al., 2014a, 2014b) or by clustering the ERT model into likely units (Ward et al., 2014). ERT inversions can also be guided by a priori information, such as from the GPR survey, to help resolve the edge of the burrows in the ERT model. The location of the interpreted burrows in the GPR radargrams can be used to constrain the ERT inversion by including boundaries in the ERT mesh (Doetsch et al., 2012; Orlando, 2013). This can be further developed using image-guided inversions where boundaries are introduced to the mesh and structure-orientated smoothing is applied by weighting the smoothing matrices favourably where there are aligned to the boundaries (Zhou et al., 2014). However, combining the GPR data with the ERT data prior to inversion has two main limitations. Firstly, ERT is no longer fully independent of the GPR results, so agreement between the ERT and GPR cannot be relied upon to determine the presence of a burrow. Secondly, Zhou et al. (2014) clip their ERT data to match the GPR's depth of investigation, this limits the depth of investigation of the ERT survey, so deeper burrows may be missed.

5.3. Management of burrowing animals in flood embankments

In the UK, disturbing burrows dug by badgers, beavers and otters is illegal without a license (DEFRA, 2022; 2014). For badgers, once a license is granted, the badgers can be evicted, and work can only begin after 21 days of no recorded activity; this makes it time consuming and expensive to remediate burrows. Integrating remote sensing and geophysical methods could enable embankment managers to detect animal burrowing earlier and monitor the locations of the burrows. Remediation could be the final option when the burrows reach a particular location or threshold within or near the embankment.

Remote sensing, such as aerial imagery, can identify areas of bare

soil excavated by the larger burrowing animals (e.g. Site 1, Fig. 3A) (Orlandini et al., 2015). To proactively monitor for burrowing activity, repeat aerial surveys with high temporal and spatial resolution would be ideal for monitoring flood embankments, but burrowing activity is visible in open-source data such as Google Imagery. Additionally, high resolution time-lapse LiDAR data (e.g. 10 cm resolution) could identify localised changes in embankment height associated with animal burrows and not be limited by tree cover.

When burrowing in or close to a flood embankment is found, its impact on the embankment should be determined. Simulations suggest that animal burrows within embankments do not uniformly impact their performance (Balistrocchi et al., 2021; Dassanayake and Mousa, 2020; Palladino et al., 2020; Taccari and van der Meij, 2016). Burrows lower in the embankment slope have a more significant effect on embankment stability due to higher water pressures (Balistrocchi et al., 2021; Taccari and van der Meij, 2016). In contrast, burrows near the embankment crest have a negligible impact regarding slope and piping failures, but the tunnels map collapse allowing localised overtopping (CIRIA et al., 2013, p. 224). Burrows starting on the riverside are of more concern (e.g. Site 2), while those on the dry side (e.g. Site 1) dug into the core can act as a toe drain stabilising the embankment slope but increasing the risk of seepage and backward erosion (Taccari and van der Meij, 2016). Balistrocchi et al. (2021) found that decreasing an embankment's residual thickness (Fig. 1B) increases the risk of failure during a flood event. Knowing the location and length of the burrow network is essential to understand their impact on the performance of the flood embankment.

To constrain the possible location of the burrows, the animal species responsible and the location and direction of burrow entrances with respect to the embankment should be determined. Animal species dig burrows with different geometries and sizes, e.g. badger burrows extend no further than 10 m from an entrance and rarely deeper than 2 m (Fischer and Dunand, 2016; Roper, 1992). This information can suggest if burrows may have entered areas most at risk or if the entrances are too far to pose a risk to the embankment, e.g. in the river toe. At both the test sites, the badger tunnel entrances were ~ 3 m from the embankment, placing the embankments at risk. At this point, carrying out a combined ERT and GPR survey could be appropriate to determine the location of the burrows if the case for remediation is unclear.

Interpreting the location of the burrows in a geophysics survey must be done with care. The end of the burrow in the geophysics data can either be the burrow termination or the detectable limit where the signal from the continuing burrow can no longer be detected. At Site 2 the GPR did not detect the whole length of the burrows as they became undetectable 4 m short of the true end. To discriminate between the true tunnel end and the detectability limit several checks can be made. Firstly, is the nearest entrance <8–10 m from the imaged burrow end? If it is, the burrow might continue. Secondly, are the tunnels imaged in the GPR data close to the detectability limit? At Site 2, the GPR could detect tunnels 1.1 m deep, the average tunnel elevation was 5 m (Fig. 10) and all five tunnels disappear close to the 6 m elevation contour, suggesting that they continue but are undetectable beyond that point (Fig. 9B). The need to find the true burrow end demonstrates the benefit of using multiple geophysical methods to see if the burrow end is supported in both data sets. Any discrepancy can be further investigated, demonstrating the value of combining ERT and GPR.

Assuming the geophysical survey can fully detect and map the burrows, it can provide several useful pieces of evidence for managing the embankment. Firstly, the map will confirm the location of the tunnels and if the burrows need to be remediated. Secondly, the maps can inform the remediation process in terms of time and resources. For example, the crest height must be maintained during remediation work, if the burrow crosses the centre line, additional planning and remediation steps will be required to maintain crest height. Thirdly, protected burrowing animals may require artificial burrows to be constructed nearby for the displaced animals (Quickfall et al., 2021). The map of the burrows could guide the design of the artificial burrows. Finally, the burrows may be found not to enter the embankment, or their location is of minimal concern. Repeat geophysical surveys could check for burrow expansion; this does not have to be a full survey but could be a single line to check that no tunnels have crossed a particular threshold.

The main limitation of this methodology is that high-resolution ERT and GPR grids, necessary to have sufficient resolution of the burrows, these are too slow to survey long embankment lengths for unknown burrows. This is particularly problematic for water-dwelling species such as beavers that can dig tunnels up to 12 m deep but often start from underwater, with no surface expression that can be visually detected (Waterschap Vallei en Veluwe et al., 2020).

6. Conclusion

In this study, two badger setts in clay-rich embankments were mapped using GPR and ERT, demonstrating that geophysics can play an essential role in managing flood embankments. Although both techniques were found to have different strengths and limitations, combining them reduced their respective limitations and provided a much more robust map of the burrow network. GPR is a quick survey technique that can investigate large areas, but its penetration depth can be limited in clay ground missing the deeper tunnels. In contrast, ERT works well in clay conditions imaging at least 1.5 m deep but requires more time to collect data, and the interpretation of tunnels can be more ambiguous.

Investigation of electrode spacing found that surveys with electrodes up to 1 m apart could detect tunnels. However, electrode spacings of 0.5 m are likely the best balance of acquisition time and area covered while maintaining a sufficient signal-to-noise ratio. If individual tunnels need to be identified or the site is very heterogenous, smaller electrode spacings will increase the chance of imaging the tunnels. To map an area of 16 m by 16 m using co-located GPR and ERT, with 32 electrodes spaced 0.5 m part along 17 parallel lines, would take two people one day using the described equipment.

This methodology does have some limitations that could be opportunities for further work. Firstly, badger tunnels are known to dig at least 2 m deep. This is likely too deep for GPR to detect in clayey soil and at the detectability limit of the currant ERT survey. Secondly, if only one technique can be used at a site, there will be much greater uncertainty in interpreting the results. Finally, only known tunnels can currently be mapped due to the relatively slow acquisition and interpretation speeds. Kilometres of the embankment cannot be surveyed to detect unknown tunnels, such as those dug by beavers, where the tunnel entrances start underwater, so they have no surface expression. Beaver numbers are increasing in parts of Western Europe and receiving legal protection (DEFRA, 2022), increasing the risk of large burrows existing undetected in the flood embankment network.

CRediT authorship contribution statement

Adrian White: Conceptualization, Data curation, Investigation, Methodology, Writing – original draft, Visualization, Writing – review & editing. **Paul Wilkinson:** Conceptualization, Methodology, Supervision, Writing – review & editing. **James Boyd:** Investigation, Software. **James Wookey:** Supervision, Writing – review & editing. **John Michael Kendall:** Conceptualization, Writing – review & editing. **Andrew Binley:** Supervision, Writing – review & editing, Resources. **Timothy Grossey:** Supervision, Writing – review & editing. **Jonathan Chambers:** Conceptualization, Funding acquisition, Supervision, Writing – review & editing.

Declaration of Competing Interest

The authors declare that they have no known competing financial interests or personal relationships that could have appeared to influence

the work reported in this paper.

Data availability

Data will be made available on request.

Acknowledgements

We would like to acknowledge John Ball for his help with the geophysical field surveys, and Oliver Kuras for guidance in presenting the work. We would also like to thank Dan Normandale, Kim Ryan and Mathew Arthur from the Environment Agency for providing the field sites and providing valuable feedback on the manuscript. This work was partly funded by a NERC GW4+ UK Doctoral Training Partnership Studentship (Grant NE/L002434/1), the BGS University Funding Initiative (S337), and the ACHILLES project (EP/R034575/1). Adrian White, Paul Wilkinson, Jonathan Chambers, and James Boyd publish with the permission of the Executive Director, British Geological Survey (UKRI-NERC). The authors are grateful to the editor and two anonymous reviewers for their comments and feedback.

Appendix A. Supplementary data

Supplementary data to this article can be found online at https://doi.org/10.1016/j.enggeo.2023.107198.

References

Allroggen, N., Booth, A.D., Baker, S.E., Ellwood, S.A., Tronicke, J., 2019. High-resolution imaging and monitoring of animal tunnels using 3D ground-penetrating radar. Near Surface Geophys. 17, 291–298. https://doi.org/10.1002/nsg.12039.

Archie, G.E., 1942. The electrical resistivity log as an aid in determining some reservoir characteristics. Transact. AIME 146, 54–62. https://doi.org/10.2118/942054-G.

Baccani, G., Bonechi, L., Bongi, M., Casagli, N., Ciaranfi, R., Ciulli, V., D'Alessandro, R., Gonzi, S., Lombardi, L., Morelli, S., Nocentini, M., Pazzi, V., Tacconi Stefanelli, C., Viliani, L., 2021. The reliability of muography applied in the detection of the animal burrows within River Levees validated by means of geophysical techniques. J. Appl. Geophys. 191 https://doi.org/10.1016/j.jappgeo.2021.104376.

Balistrocchi, M., Moretti, G., Ranzi, R., Orlandini, S., 2021. Failure probability analysis of levees affected by mammal bioerosion. Water Resour. Res. 57, 1–24. https://doi.org/10.1029/2021wr030559.

Ball, J., Chambers, J., Wilkinson, P., Binley, A., 2022. Resistivity imaging of river embankments: 3D effects due to varying water levels in tidal rivers. Near Surf. Geophys. https://doi.org/10.1002/nsg.12234.

Bièvre, G., Oxarango, L., Günther, T., Goutaland, D., Massardi, M., 2018. Improvement of 2D ERT measurements conducted along a small earth-filled dyke using 3D topographic data and 3D computation of geometric factors. J. Appl. Geophys. 153, 100–112. https://doi.org/10.1016/j.jappgeo.2018.04.012.

Binley, A., Slater, L., 2020. Resistivity and Induced Polarization: Theory and applications to the Near-Surface Earth. Cambridge University Press. https://doi.org/10.1017/9781108685955.

Blanchy, G., Saneiyan, S., Boyd, J., McLachlan, P., Binley, A., 2020. ResIPy, an intuitive open source software for complex geoelectrical inversion/modeling. Comput. Geosci. 137 https://doi.org/10.1016/j.cageo.2020.104423.

Booth, A., 2019. Feasibility of Ground Penetrating Radar (GPR) Methods to Detect and Image Beaver Tunnels - Results of Field Trials around the River Isla (Perthshire).

Borgatti, L., Forte, E., Mocnik, A., Zambrini, R., Cervi, F., Martinucci, D., Pellegrini, F., Pillon, S., Prizzon, A., Zamariolo, A., 2017. Detection and characterization of animal burrows within river embankments by means of coupled remote sensing and geophysical techniques: Lessons from River Panaro (northern Italy). Eng. Geol. 226, 277–289. https://doi.org/10.1016/j.enggeo.2017.06.017.

Browne, E., Driessen, M.M., Ross, R., Roach, M., Carver, S., 2021. Environmental suitability of bare-nosed wombat burrows for Sarcoptes scabiei. Int J Parasitol Parasites Wildl 16, 37–47. https://doi.org/10.1016/j.ijppaw.2021.08.003.

Burke, M.J., Brennand, T.A., Perkins, A.J., 2012. Transient subglacial hydrology of a thin ice sheet: Insights from the Chasm esker, British Columbia, Canada. Quat. Sci. Rev. 58, 30–55. https://doi.org/10.1016/j.quascirev.2012.09.004.

Butler, J., Roper, T.J., Clark, A.J., 1994. Investigation of badger (Meles meles) setts using soil resistivity measurements. J. Zool. 232, 409–418. https://doi.org/10.1111/j.1469-7998.1994.tb01582.x.

Byrne, A.W., Paddy Sleeman, D., O'Keeffe, J., Davenport, J., 2012. The ecology of the European badger (*Meles meles*) in Ireland: a review. Biol. Enviro. Proceedi. Royal Irish Acad. 112, 105–132. https://doi.org/10.3318/BIOE.2012.02.

Carrière, S.D., Chalikakis, K., Sénéchal, G., Danquigny, C., Emblanch, C., 2013. Combining electrical resistivity tomography and ground penetrating radar to study geological structuring of karst unsaturated zone. J. Appl. Geophys. 94, 31–41. https://doi.org/10.1016/j.jappgeo.2013.03.014.

Ceccato, F., Malvestio, S., Simonini, P., 2022. Effect of animal burrows on the vulnerability of levees to concentrated erosion. Water (Basel) 14, 2777. https://doi.org/10.3390/w14182777.

Chambers, J.E., Wilkinson, P.B., Wardrop, D., Hameed, A., Hill, I., Jeffrey, C., Loke, M. H., Meldrum, P.I., Kuras, O., Cave, M., Gunn, D.A., 2012. Bedrock detection beneath river terrace deposits using three-dimensional electrical resistivity tomography. Geomorphology 177–178, 17–25. https://doi.org/10.1016/j.geomorph.2012.03.034.

Chambers, J.E., Gunn, D.A., Wilkinson, P.B., Meldrum, P.I., Haslam, E., Holyoake, S., Kirkham, M., Kuras, O., Merritt, A., Wragg, J., 2014a. 4D electrical resistivity tomography monitoring of soil moisture dynamics in an operational railway embankment. Near Surface Geophys. 12, 61–72. https://doi.org/10.3997/1873-0604.2013002.

Chambers, J.E., Wilkinson, P.B., Uhlemann, S., Sorensen, J.P.R., Roberts, C., Newell, A. J., Ward, W.O.C., Binley, A., Williams, P.J., Gooddy, D.C., Old, G., Bai, L., 2014b. Derivation of lowland riparian wetland deposit architecture using geophysical image analysis and interface detection. Water Resour. Res. 50, 5886–5905. https://doi.org/10.1002/2014WR015643.

Chlaib, H.K., Mahdi, H., Al-Shukri, H., Su, M.M., Catakli, A., Abd, N., 2014. Using ground penetrating radar in levee assessment to detect small scale animal burrows. J. Appl. Geophys. 103, 121–131. https://doi.org/10.1016/j.jappgeo.2014.01.011.

CIRIA, Ministry of Ecology, USACE, 2013. The International Levee Handbook. CIRIA.

Cortez, J.D., Henke, S.E., Redeker, E., Fulbright, T.E., Riddle, R., Young, J., 2013. Demonstration of ground-penetrating radar as a useful tool for assessing pocket gopher burrows. Wildl. Soc. Bull. 37, 428–432. https://doi.org/10.1002/wsb.279.

Dahlin, T., Zhou, B., 2004. A numerical comparison of 2D resistivity imaging with 10 electrode arrays. Geophys. Prospect. 52, 379–398. https://doi.org/10.1111/j.1365-2478.2004.00423.x.

Dassanayake, S.M., Mousa, A., 2020. Probabilistic stability evaluation for wildlife-damaged earth dams: a Bayesian approach. Georisk 14, 41–55. https://doi.org/10.1080/17499518.2018.1542499.

DEFRA, 2014. Badgers: Protection and Licences [WWW Document]. URL. https://www.gov.uk/guidance/badgers-protection-surveys-and-licences (accessed 1.9.23).

DEFRA, 2022. Protection and Management of Beavers in England [WWW Document]. URL. https://www.gov.uk/government/publications/beavers-protection-and-management/protection-and-management-of-beavers-in-england (accessed 1.9.23).

Doetsch, J., Linde, N., Pessognelli, M., Green, A.G., Günther, T., 2012. Constraining 3-D electrical resistance tomography with GPR reflection data for improved aquifer characterization. J. Appl. Geophys. 78, 68–76. https://doi.org/10.1016/j.jappgeo.2011.04.008.

Dunbar, J.B., Llopis, J.L., Sills, G.L., Smith, E.W., Miller, R.D., Ivanov, J., Corwin, R.F., 2007. Condition assessment of levees, U.S. section of the international boundary and water commission. In: Report 5: Flood simulation Study of Retamal Levee, lower Rio Grande Valley, Texas, Using Seismic and Electrical Geophysical Models.

Dyer, M., Gardener, R., 1996. Geotechnical Performance of Flood Defence Embankments: Scoping Study. Environment Agency.

Environment Agency, 2015. Humber FCRM Strategy – Humber Defence Condition & Fragility. An Investigation into the Performance of the Humber Flood Embankments. Short Report:. Alkborough Flats Badger Sett.

Environment Agency, 2016. Impact Report Winter Flooding 2015–16.

Fischer, C., Dunand, F., 2016. 3D topography and structure analysis of three European badger (Meles meles) setts from western Switzerland. Wildl. Biol. Pract. 12, 26–35. https://doi.org/10.2461/wbp.2016.eb.3.

Ford, J.R., Kessler, H., Price, S.J., Hall, M., Cooper, A.H., 2004. Field guide to the glacial evolution of the Vale of York. In: British Geological Survey Internal Report, IR/04/106.

Gharibi, M., Bentley, L.R., 2005. Resolution of 3-D electrical resistivity images from inversions of 2-D orthogonal lines. J. Environ. Eng. Geophys. 10, 339–349. https://doi.org/10.2113/JEEG10.4.339.

Gilvear, D.J., Black, A.R., 1999. Flood-induced embankment failures on the river tay: Implications of climatically induced hydrological change in Scotland. Hydrol. Sci. J. 44, 345–362. https://doi.org/10.1080/02626669909492231.

Günther, T., Rücker, C., Spitzer, K., 2006. Three-dimensional modelling and inversion of dc resistivity data incorporating topography – II. Inversion. Geophys. J. Int. 166, 506–517. https://doi.org/10.1111/j.1365-246X.2006.03011.x.

Hojat, A., Arosio, D., Ivanov, V.I., Loke, M.H., Longoni, L., Papini, M., Tresoldi, G., Zanzi, L., 2020. Quantifying seasonal 3D effects for a permanent electrical resistivity tomography monitoring system along the embankment of an irrigation canal. Near Surface Geophys. 18, 427–443. https://doi.org/10.1002/nsg.12110.

IPCC, 2014. Climate change 2014: impacts, adaptation, and vulnerability. part a: global and sectoral aspects. In: Contribution of Working Group II to the Fifth Assessment Report of the Intergovernmental Panel on Climate Change. Cambridge University Press, Cambridge, United Kingdom and New York, NY, USA.

Jol, H.M., 2009. Ground Penetrating Radar Theory and Applications. Elsevier. https://doi.org/10.1016/B978-0-444-53348-7.X0001-4.

Kinlaw, A., Grasmueck, M., 2012. Evidence for and geomorphologic consequences of a reptilian ecosystem engineer: the burrowing cascade initiated by the Gopher Tortoise. Geomorphology 157–158, 108–121. https://doi.org/10.1016/j.geomorph.2011.06.030.

Leslie, I.N., Heinse, R., 2013. Characterizing soil-pipe networks with pseudo-three-dimensional resistivity tomography on forested hillslopes with restrictive horizons. Vadose Zone J. 12, 1–10. https://doi.org/10.2136/vzj2012.0200.

Loke, M.H., Chambers, J.E., Rucker, D.F., Kuras, O., Wilkinson, P.B., 2013. Recent developments in the direct-current geoelectrical imaging method. J. Appl. Geophys. 95, 135–156. https://doi.org/10.1016/j.jappgeo.2013.02.017.

Macdonald, D.W., Newman, C., Dean, J., Buesching, C.D., Johnson, P.J., 2004. The distribution of Eurasian badger, Meles meles, setts in a high-density area: field observations contradict the sett dispersion hypothesis. Oikos 106, 295–307. https://doi.org/10.1111/j.0030-1299.2004.12879.x.

Martínez-Pagán, P., Gómez-Ortiz, D., Martín-Crespo, T., Manteca, J.I., Rosique, M., 2013. The electrical resistivity tomography method in the detection of shallow mining cavities. A case study on the Victoria Cave, Cartagena (SE Spain). Eng. Geol. 156, 1–10. https://doi.org/10.1016/j.enggeo.2013.01.013.

Nichol, D., Lenham, J.W., Reynolds, J.M., 2003. Application of ground-penetrating radar to investigate the effects of badger setts on slope stability at St Asaph Bypass, North Wales. Q. J. Eng. Geol. Hydrogeol. 36, 143–153. https://doi.org/10.1144/1470-9236/2002-42.

Orlandini, S., Moretti, G., Albertson, J.D., 2015. Evidence of an emerging levee failure mechanism causing disastrous floods in Italy. Water Resour. Res. 51, 7995–8011. https://doi.org/10.1002/2015WR017426.

Orlando, L., 2013. GPR to constrain ERT data inversion in cavity searching: Theoretical and practical applications in archeology. J. Appl. Geophys. 89, 35–47. https://doi.org/10.1016/j.jappgeo.2012.11.006.

Palladino, M.R., Barbetta, S., Camici, S., Claps, P., Moramarco, T., 2020. Impact of animal burrows on earthen levee body vulnerability to seepage. J Flood Risk Manag 13, 1–21. https://doi.org/10.1111/jfr3.12559.

Pellicer, X.M., Warren, W.P., Gibson, P., Linares, R., 2012. Construction of an evolutionary deglaciation model for the Irish midlands based on the integration of morphostratigraphic and geophysical data analyses. J. Quat. Sci. 27, 807–818. https://doi.org/10.1002/jqs.2570.

Quickfall, L., Richardson, A., Summers, L., 2021. Recovery works - River embankment repairs across East Lindsey. In: ADA Gazette, 16.

Reading, H.G., 1986. Sedimentary Environments and Facies, 2nd ed. Blackwell scientific publications.

Remonti, L., Balestrieri, A., Prigioni, C., 2006. Factors determining badger Meles meles sett location in agricultural ecosystems of NW Italy. Folia Zool Brno 55, 19–27.

Reynolds, J.M., 2011. An Introduction to Applied and Environmental Geophysics. John Wiley & Sons.

Roper, T.J., 1992. Badger *Meles meles* setts–architecture, internal environment and function. Mammal Rev. 22, 43–53. https://doi.org/10.1111/j.1365-2907.1992.tb00118.x.

Roper, T.J., Tait, A.I., Fee, D., Christian, S.F., 1991. Internal structure and contents of three badger (*Meles meles*) setts. J. Zool. 225, 115–124. https://doi.org/10.1111/j.1469-7998.1991.tb03805.x.

RSK, 2020. A Reference for Geophysical Techniques and Applications, 4th edition.

Saey, T., van Meirvenne, M., de Pue, J., van de Vijver, E., Delefortrie, S., 2014. Reconstructing mole tunnels using frequency-domain ground penetrating radar. Appl. Soil Ecol. 80, 77–83. https://doi.org/10.1016/j.apsoil.2014.03.019.

Satriani, A., Loperte, A., Proto, M., Bavusi, M., 2010. Building damage caused by tree roots: laboratory experiments of GPR and ERT surveys. Adv. Geosci. 24, 133–137. https://doi.org/10.5194/adgeo-24-133-2010.

Stott, P., 1996. Ground-penetrating radar: a technique for investigating the burrow structures of fossorial vertebrates. Wildl. Res. 23, 519. https://doi.org/10.1071/WR9960519.

Swinbourne, M.J., Taggart, D.A., Sparrow, E., Hatch, M., Ostendorf, B., 2015. Ground penetrating radar as a non-invasive tool to better understand the population dynamics of a fossorial species: mapping the warrens of southern hairy-nosed wombats (Lasiorhinus latifrons). Wildl. Res. 42, 678–688. https://doi.org/10.1071/WR15068.

Swinbourne, M.J., Taggart, D., Ostendorf, B., 2016. Non-Invasive Exploration of Underground Wombat Tunnels, 1–3. The International Society for Optics and Photonics Newsroom. https://doi.org/10.1117/2.1201604.006452.

Taccari, M.L., van der Meij, R., 2016. Study of the effect of burrows of European Badgers (*Meles meles*) on the initiation of breaching in dikes. E3S Web Conf. 7, 7. https://doi.org/10.1051/e3sconf/20160703001.

Tellman, B., Sullivan, J.A., Kuhn, C., Kettner, A.J., Doyle, C.S., Brakenridge, G.R., Erickson, T.A., Slayback, D.A., 2021. Satellite imaging reveals increased proportion of population exposed to floods. Nature 596, 80–86. https://doi.org/10.1038/s41586-021-03695-w.

Tresoldi, G., Arosio, D., Hojat, A., Longoni, L., Papini, M., Zanzi, L., 2019. Long-term hydrogeophysical monitoring of the internal conditions of river levees. Eng. Geol. 259, 1–11. https://doi.org/10.1016/j.enggeo.2019.05.016.

Tso, C.H.M., Kuras, O., Wilkinson, P.B., Uhlemann, S., Chambers, J.E., Meldrum, P.I., Graham, J., Sherlock, E.F., Binley, A., 2017. Improved characterisation and modelling of measurement errors in electrical resistivity tomography (ERT) surveys. J. Appl. Geophys. 146, 103–119. https://doi.org/10.1016/j.jappgeo.2017.09.009.

Virgós, E., Casanovas, J.G., 1999. Badger Meles meles sett site selection in low density Mediterranean areas of Central Spain. Acta Theriol (Warsz) 44, 173–182. https://doi.org/10.4098/AT.arch.99-15.

Ward, W.O.C., Wilkinson, P.B., Chambers, J.E., Oxby, L.S., Bai, L., 2014. Distribution-based fuzzy clustering of electrical resistivity tomography images for interface detection. Geophys. J. Int. 197, 310–321. https://doi.org/10.1093/gji/ggu006.

Waterschap Vallei en Veluwe, 2020. Waterschap Rijn en IJssel, Waterschap Hollandse Delta, Waterschap Rivierenland, Hoogheemraadschap De Stichtse Rijnlanden, Hoogheemraadschap Amstel, G. en V., Provincie Gelderland, Provincie Zuid-Holland, Unie van Waterschappen (Beverprotocol voor de waterbeheerders in de provincies Gelderland en Zuid-Holland).

Waxman, M.H., Smits, L.J.M., 1968. Electrical Conductivities in Oil-Bearing Shaly Sands. Soc. Pet. Eng. J. 8, 107–122. https://doi.org/10.2118/1863-A.

Wilkinson, P.B., Meldrum, P.I., Chambers, J.E., Kuras, O., Ogilvy, R.D., 2006. Improved strategies for the automatic selection of optimized sets of electrical resistivity tomography measurement configurations. Geophys. J. Int. 167, 1119–1126. https://doi.org/10.1111/j.1365-246X.2006.03196.x.

Wilkinson, P.B., Inauen, C.M., Uhlemann, S.S., Swift, R.T., Dashwood, B., 2018. Geophysical Investigations to Determine the Structure of a Badger Sett in a Flood Embankment.

Wisniewski, K.D., Pringle, J.K., Allen, D., Wilson, G.E., 2019. Wildlife crime: the application of forensic geoscience to assist with criminal investigations. Forensic Sci. Int. 294, e11–e18. https://doi.org/10.1016/j.forsciint.2018.10.026.

Xu, X., Zeng, Q., Li, D., Wu, J., Wu, X., Shen, J., 2010. GPR detection of several common subsurface voids inside dikes and dams. Eng. Geol. 111, 31–42. https://doi.org/10.1016/j.enggeo.2009.12.001.

Zhou, J., Revil, A., Karaoulis, M., Hale, D., Doetsch, J., Cuttler, S., 2014. Image-guided inversion of electrical resistivity data. Geophys. J. Int. 197, 292–309. https://doi.org/10.1093/gji/ggu001.